On the bonding of small group 12 clusters

H.-J. Flad[1,a], F. Schautz[1], Yixuan Wang[1,b], M. Dolg[1], and A. Savin[2]

[1] Max-Planck-Institut für Physik komplexer Systeme, Nöthnitzer Str. 38, 01187 Dresden, Germany
[2] Laboratoire de Chimie Théorique (CNRS), Université Pierre et Marie Curie 4, place Jussieu, 75252 Paris, France

Abstract. Characteristic properties as well as possible differences in bonding of small group 12 clusters M_n (M = Zn, Cd, Hg; $n = 2, \ldots, 6$) have been investigated by quantum chemical *ab initio* methods, *i.e.*, relativistic large-core pseudopotentials, core-polarization potentials and coupled-cluster correlation treatments. A comparison of cohesive energies and spectroscopic properties like ionization potentials, electron affinities, and vibrational frequencies reveals a close similarity between the clusters of Cd and Hg. For Zn clusters we observed an exceptional increase in stability between Zn_3 and Zn_4. In order to get a more qualitative picture of the covalent contributions to bonding we have calculated the electron localization function (ELF). The ELF analysis is in accordance with the calculated spectroscopic properties and shows predominant van der Waals interactions with weak covalent contributions for all the cluster sizes considered.

PACS. 36.40.-c Atomic and molecular clusters

1 Introduction

The clusters of group 12 elements (Zn, Cd, Hg) deserve special attention among the elemental clusters since they cover the whole spectrum from van der Waals interaction to covalent and finally metallic types of chemical bonding. The changes in bonding with increasing cluster size are mainly associated to the closing of the gap between the molecular orbitals resulting from the atomic s- and p-type valence orbitals. The size dependence of this transition for neutral clusters has been studied experimentally for Cd [1–3] and Hg [4–16] clusters. The most important accessible property indicating this transition is the ionization potential (IP) which can be measured by photoionization [1,6] or electron-impact ionization [4,10] mass spectroscopy. Furthermore photoelectron [2,13], inner-shell autoionization spectra [5,7] and optical-absorption cross-sections [14] have been reported in the literature. The interpretation of the experimental results concerning the exact onset of covalent and metallic bonding is still controversial [6,10], however, there is an agreement that the transition between covalent and metallic bonding takes place between 13 and 90 atoms.

Due to the availability of numerous experimental results for mHg clusters these systems have also attracted considerable interest from the theoretical point of view [17–20]. Most of the work is based on model Hamiltonians [17–19] which have the advantage to permit calculations over

a large range of cluster sizes. The severe problem of this approach is that it requires some *a priori* knowledge of the system in order to determine the interaction terms of the model and the effective parameters belonging to it. Due to changes in the character of the bonding the model also has to change in order to reproduce the experimental results [18]. Other first principles approaches based on uncorrelated wave functions [20] or density functional theory [21] (DFT) are problematic due to different reasons. It is well known that electron correlation is very important for a reasonable description of systems interacting predominantly via van der Waals forces and has to be included in *ab initio* calculations. Although DFT accounts for electron correlation, it encounters problems for van der Waals type interactions. Depending on the chosen functional and system it may over- or under-estimate the binding energy [22]. A good starting point for a systematic discussion of the performance of various *ab initio* methods are the group 12 dimers. Previous work [23–26] suggests a combination of large-core relativistic pseudopotentials (PP) including a core-polarization potential (CPP) together with a size-extensive high-quality correlation treatment using large and flexible valence basis sets. The application of large-core PPs deserves some care, especially in the case of strong covalent or ionic interactions which have significant influence on the underlying d shell. In the present application the interactions are still rather weak and the core-valence correlation is reasonably well described by the polarization potential. Since the PPs have been adjusted to reproduce the splitting between the s and p valence orbitals, we would expect that the results

---

[a] e-mail: `flad@mpipks-dresden.mpg.de`
[b] On leave from Shandong University, Jinan, People's Republic of China.

are reasonable even for much larger clusters. Currently the limitations are mainly due to the required large basis sets restricting the calculations to clusters with up to 15 atoms.

In the present work we are mainly interested in the transition between van der Waals and covalent bonding. There is experimental evidence [3] that this transition occurs faster for Cd than for Hg clusters. For this reason we have performed a comparative study for small group 12 cluster with up to 6 atoms. The limitation with respect to the number of atoms is due to the high demands concerning the correlation method and the basis sets. The necessity of size-extensivity suggests the application of the coupled-cluster (CC) method including all single and double excitations explicitly as well as a pertubative treatment of the triple excitations (CCSD(T)). This method has been applied sucessfully to group 12 dimers [23–26] and Hg clusters [27]. In our previous work [27] we have also employed the quantum Monte Carlo (QMC) method which yields an excellent agreement with CC results for the cluster sizes considered. Since we were interested in the vibrational frequencies of the clusters, we decided to use only the CC method. The required second derivatives along nuclear displacement coordinates can be obtained from CC calculations by straightforward numerical differentiation using total energies from nearby coordinates. QMC energies are always afflicted with statistical uncertainties which make the evaluation of such derivatives more complicated.

2 Results and discussion

2.1 Structures, cohesive energies and the electron localization function

The accurate determination of equilibrium structures for the clusters under consideration is a basic requirement for the discussion of their properties and the variation of the chemical bond with the cluster size. There may exist various possible structures for a given number of atoms which are rather close in energy. It is therefore important to estimate the sensitivity of a given property with respect to structural changes. Unfortunately no experimental information on the structure of small group 12 clusters is available. Molecular beam experiments are performed with hot clusters, as a consequence the measured properties do not reveal a resolution with respect to different structures. Well-defined equilibrium structures cannot be obtained from such experiments, a fact which should be kept in mind when comparing the results of calculations with experiment. New experimental developments for the generation of cold clusters [28] may improve the situation considerably.

Locating the equilibrium structure using *ab initio* quantum chemistry methods requires a significant computational effort due to its strong dependence on electron correlation. We restricted ourselves to highly symmetrical, densely packed structures which seem to be the most natural ones for systems with predominantly van der Waals
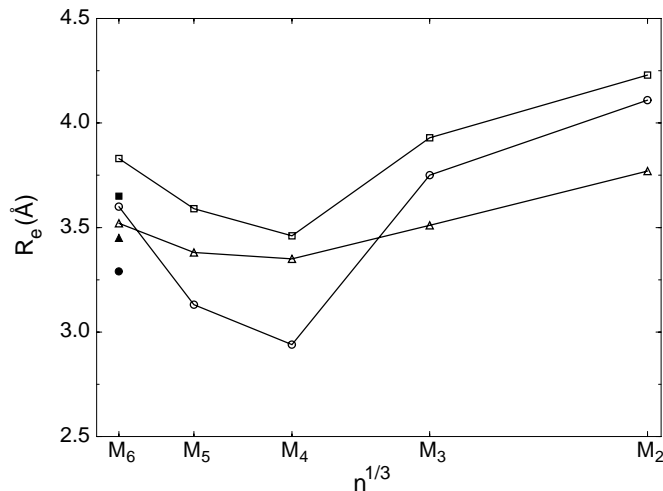

Fig. 1. Averaged bond length (Å) per nearest-neighbor interaction for Zn $\bigcirc$, Cd $\square$ and Hg $\triangle$. The filled symbols refer to the bicapped tetrahedral structure of M_6.
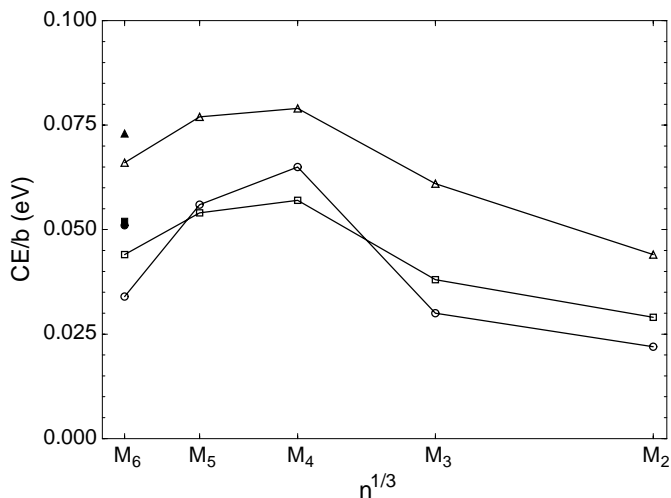
Fig. 2. Cohesive energy per nearest-neighbor interaction for Zn $\bigcirc$, Cd $\square$ and Hg $\triangle$. The filled symbols refer to the bicapped tetrahedral structure of M_6.

type of interactions. This includes equilateral triangular ($n = 3$), tetrahedral ($n = 4$), trigonal bipyramidal ($n = 5$), and octahedral ($n = 6$) structures. In order to jugde whether or not a given structure is a real minimum with respect to unconstrained variations of the shape of the structure, we have performed a normal coordinate analysis. Any distortion of the minimum energy structure from perfect symmetry would have been detected at this stage since it leads to an imaginary frequency. Strictly speaking, we proved that the structures represent local minima but we cannot rule out the possibility that the global minima corresponds to a different structure. Actually for $n = 6$ we have detected a bicapped tetrahedral structure lower in energy, as it will be discussed below. For the clusters with $n = 3, 4, 5$ our choices are the ones with the maximum number of nearest-neighbor interactions and the densest packing of the atoms. In our opinion this is a

Table 1. Bond lengths R_e (Å), ionization potentials IP (eV), electron affinities EA (eV), cohesive energies per atom CE (eV), harmonic vibrational frequencies ω_e (cm^{-1}) for the equilateral triangular structure obtained from coupled-cluster (CC) calculations. The corresponding values obtained with the optimized model potentials (MP) are listed for comparison. The averaged vibrational frequency $\overline{\omega}$ is given for both cases.

	Zn$_3$		Cd$_3$		Hg$_3$	
	CC	MP	CC	MP	CC	MP
R_e	3.75	3.75	3.93	3.93	3.51	3.51
IP	8.25		7.93		9.08	
EA	a		a		0.13	
CE	0.030	0.030	0.038	0.041	0.061	0.061
$\omega_{A_1'}$	25.8	33.7	22.7	27.8	28.3	39.0
$\omega_{E'}$	29.4	23.8	23.3	19.7	35.1	27.6
$\overline{\omega}$	28.2	27.1	23.1	22.4	32.8	31.4

a Anion not stable in CCSD(T) calculations.

Table 2. As in Table 1 but for the tetrahedral structure.

	Zn$_4$		Cd$_4$		Hg$_4$	
	CC	MP	CC	MP	CC	MP
R_e	2.94	2.93	3.46	3.46	3.35	3.35
IP	7.77		7.61		8.94	
EA	0.62		0.55		0.39	
CE	0.097	0.097	0.085	0.086	0.118	0.118
ω_{A_1}	76.6	111.5	39.5	57.5	42.5	51.0
ω_E	78.1	55.7	39.4	28.7	31.1	25.5
ω_{T_2}	84.7	78.8	44.1	40.6	37.4	36.0
$\overline{\omega}$	81.2	76.6	41.8	39.5	36.2	35.0

Table 3. As in Table 1 but for the trigonal bipyramidal structure.

	Zn$_5$		Cd$_5$		Hg$_5$	
	CC	MP	CC	MP	CC	MP
R_q	2.89	3.23	3.41	3.56	3.25	3.35
R_x	3.25	3.22	3.68	3.55	3.44	3.35
IP	7.29		7.23		8.36	
EA	0.62		0.61		0.50	
CE	0.100	0.089	0.097	0.91	0.139	0.136
$\omega_{A_1'}$	86.3	85.8	45.7	50.6	52.5	52.1
	55.4	49.0	34.3	28.7	33.8	29.6
$\omega_{E'}$	85.9	59.7	45.1	35.2	42.8	36.2
	38.9	32.4	23.3	19.1	21.8	19.7
$\omega_{A_2''}$	26.7	76.3	27.2	45.3	34.3	46.5
$\omega_{E''}$	54.5	56.7	33.4	33.7	31.8	34.5
$\overline{\omega}$	58.6	56.5	34.5	33.4	34.8	34.3

convincing argument that these structures represent global minima. This argument is also in line with our results for $n = 6$ where the octahedral and bicapped tetrahedral structures have the same number of nearest-neighbor interactions but the latter possesses the denser packing. The size dependences of averaged bond length and cohesive energy per nearest-neighbor interaction (CE/b) are shown in Figures 1 and 2, the exact numbers are listed in Tables 1 to 4. For all group 12 elements we obtain a local minimum (maximum) with respect to the bond length (CE/b) for the tetrahedral structure. It is most pronounced for Zn$_4$ and becomes more and more shallow for Cd$_4$ and Hg$_4$. There is a corresponding strong increase for Zn$_4$ in the CE/b between the equilateral triangular and tetrahedral structure. Looking at the trigonal bipyramidal structure in more detail we find in all three cases a significant difference beween the equatorial and axial bond lengths. For Zn$_5$ and Cd$_5$ the equatorial bond lengths are close to that of the tetrahedral structures whereas the axial bond lengths are longer by 0.36 Å, respectively, 0.27 Å. This result indicates a noticeable increase of the covalent contribution to the bonding in the tetrahedral and the equatorial region of the trigonal bipyramidal structures for Zn and Cd. The large increase of the bond lengths for the octahedral structure is due to the fact that the packing is less dense there. We have calculated an alternative structure for $n = 6$ which consists of a bicapped tetrahedron resembling more closely the packing of the preceding ones. Actually, the averaged bond lengths decreased considerably for Zn and Cd together with an increasing CE/b for all three elements.

In order to get a better insight into the covalent contributions to the bonding we have used the electron localization function [29,30] (ELF) as a tool to visualize the electronic structure of the clusters. Given an electron at a point $\vec{r}$, ELF is a measure for the conditional probability to find a second electron with parallel spin close to it. Starting from the spherically averaged pair spin density

$P_{\sigma\sigma}(\vec{r}, s)$ (s electron-electron distance) Becke and Edgecombe [29] performed a Taylor expansion with respect to s:

$$P_{\sigma\sigma}(\vec{r}, s) = \frac{1}{2} D_{\sigma\sigma}(\vec{r}) s^2 \ldots \qquad (1)$$

with the second-order term for a closed shell Hartree-Fock (HF) wave function given by

$$D_{\sigma\sigma}(\vec{r}) = \sum_i |\nabla \phi_{i\sigma}(\vec{r})|^2 - \frac{1}{4} \frac{|\nabla \rho_\sigma(\vec{r})|^2}{\rho_\sigma}, \qquad (2)$$

where i runs over all σ spin orbitals $\phi_{i\sigma}$. The second order probability $D_{\sigma\sigma}$ is scaled with the corresponding probability for a homogeneous electron gas $\overline{D}_{\sigma\sigma}$ of the same local density,

$$\text{ELF} = \left\{ 1 + \left[\frac{D_{\sigma\sigma}(\vec{r})}{\overline{D}_{\sigma\sigma}(\vec{r})} \right]^2 \right\}^{-1}. \qquad (3)$$

By construction ELF can adopt values in the interval $[0, 1]$ and with increasing ELF value the probability for a second electron with parallel spin to be close to the reference

Table 4. As in Table 1 but for the octahedral structure. The numbers in parentheses belong to the bicapped tetrahedral structure (bond lengths refer to an edge of the tetrahedron, respectively, the distance between vertex and surface atom).

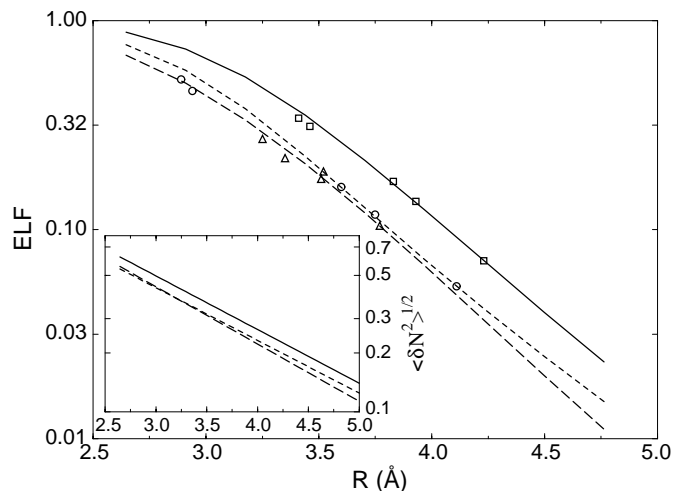|	Zn_6		Cd_6		Hg_6	
	CC	MP	CC	MP	CC	MP
R_e	3.60 (3.03, 3.55)	3.60	3.83 (3.51, 3.80)	3.83	3.52 (3.39, 3.52)	3.52
IP	7.32 (7.13)		7.07 (7.04)		8.12 (8.25)	
EA	0.73 (0.69)		0.80 (0.70)		0.77 (0.58)	
CE	0.068 (0.101)	0.066	0.087 (0.104)	0.085	0.132 (0.145)	0.132
$\omega_{A_{1g}}$	37.1	37.9	32.5	32.7	37.4	36.0
ω_{E_g}	17.9	16.8	15.0	14.6	16.4	16.2
$\omega_{T_{2g}}$	28.3	27.8	24.2	23.9	25.9	26.2
$\omega_{T_{1u}}$	26.0	33.6	24.7	29.0	28.9	31.9
$\omega_{T_{2u}}$	30.8	18.9	23.1	16.4	22.5	18.1
$\overline{\omega}$	27.4	26.0	23.2	22.5	25.2	24.8

Fig. 3. The value of the electron localization function (ELF) at the center of the group 12 dimers *versus* the interatomic distance (Å) (Zn_2 short-dashed line, Cd_2 solid line, Hg_2 long-dashed line) together with the ELF values at the saddle points of the clusters at the corresponding bond distances (Zn ○, Cd □, Hg △). The inset is taken from reference [26] and shows the corresponding charge fluctuations.

electron decreases. It is therefore a measure for the localization of electrons since in the case that the reference electron represents a localized electron the probability for a second electron to be close to it decreases with increasing localization. Maxima of ELF locate the regions which can be interpreted as bonds, lone pairs, cores etc. It has been sucessfully applied to study the shell structure of atoms and the chemical bonding in molecules and solids (for a recent review with extensive bibliography see Savin *et al.* [31]). For a pure van der Waals type of bonding ELF exhibits a deep saddle point between the atoms. If the reference electron is between the atoms it has a highly localized electron with parallel spin in its neighborhood which strongly increases the probability of approaching each other compared to the homogeneous electron gas.

The depth at the saddle point is a measure for the covalency of the interaction. We have chosen the group 12 dimers as a reference.

As already discussed above, the inclusion of electron correlation is essential for a correct description of group 12 clusters. Although ELF is based on the HF wave function it can give some useful information, since the structures have been optimized on the correlated level. Therefore correlation effects enter indirectly into ELF. This resembles some similarities with our previous work on group 12 dimers [25,26] where we have used charge fluctuations to define the covalent contributions. A comparison of charge fluctuations from QMC and HF calculations revealed no significant correlation contributions. Over a large range of interatomic distances the charge fluctuations showed a nearly linear behavior on a logarithmic scale. In Figure 3 we have plotted the ELF values for the dimers at the center of the bond over a range of interatomic distances. A comparison of these curves with the corresponding curves for the charge fluctuations shows an amazing similarity. The curves for Zn_2 and Hg_2 are close together and Cd_2 is above them. Furthermore we have indicated in Figure 3 the ELF value at the saddle points of the clusters at the corresponding bond distance. They are in good agreement with those of the dimers at these bond distances. Therefore it exists an almost quantitative relation between the atomic distance and the covalent contributions to bonding. Figure 4a shows the Zn dimer for which ELF has a deep saddle point between the atoms. The ELF for the other group 12 dimers shows a similar behavior. A comparison of ELF for Zn_2 and Zn_3 (Fig. 4b) shows a slight flattening of the saddle point for Zn_3 but the qualitative picture remains the same. Again Cd and Hg behave similarly. However, the ELF for the tetrahedral structure of the group 12 elements exhibits characteristic differences. In accordance with the observed trends for the bond distance and CE we observe a strong increase of ELF in the interatomic region for Zn_4 (Fig. 4c) and a tiny one for Hg_4 with Cd_4 (Figs. 4d,e) in between. The maximum increase is not on the interatomic axis but somewhat beside
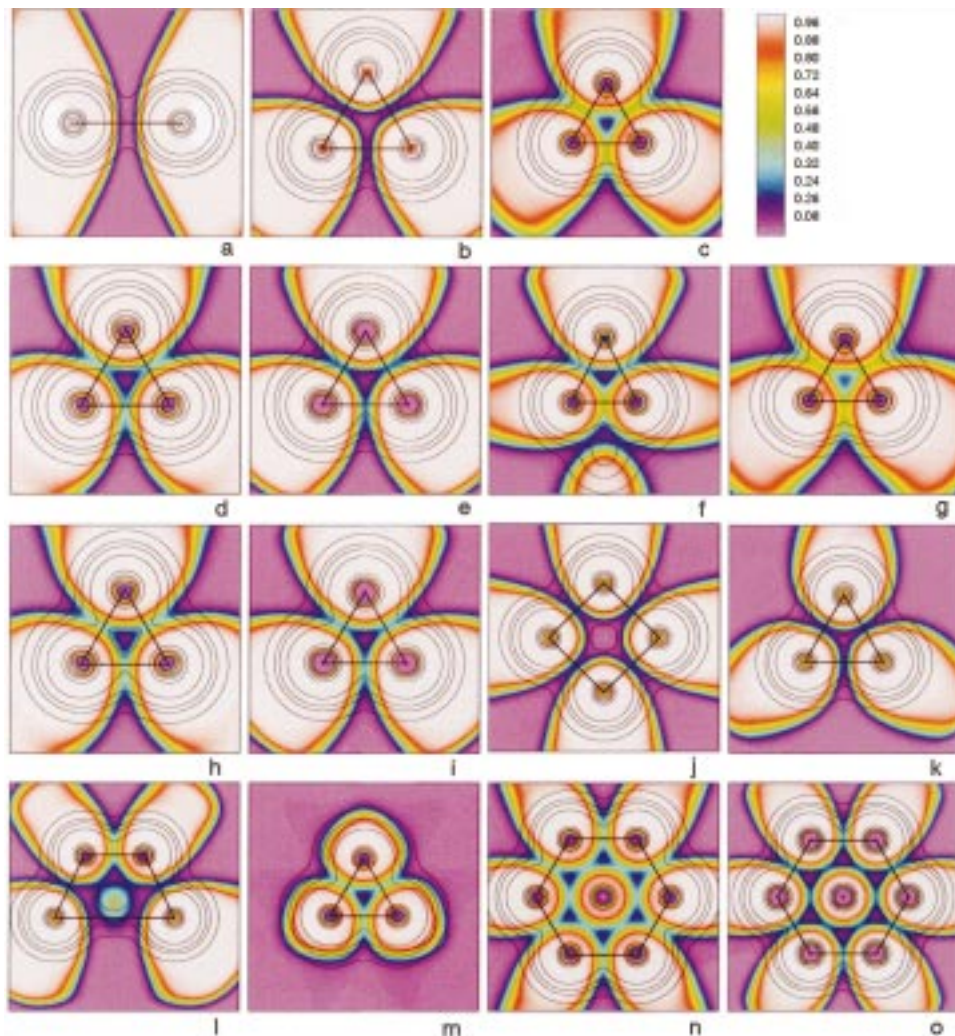
Fig. 4. 2D plots of ELF for selected structures and elements. The ELF values are encoded by colors superposed with contour lines representing the electron density to indicate the size of the cluster. Dimer, a) Zn_2; equilateral triangular structure b) Zn_3; surface of the tetrahedral structure, c) Zn_4, d) Cd_4, e) Hg_4; section through an axial and two equatorial atoms of the trigonal bipyramidal structure, f) Zn_5; section through the equatorial plane of the trigonal bipyramidal structure, g) Zn_5, h) Cd_5, i) Hg_5; section through four atoms of the octahedral structure j) Zn_6; surface of the octahedral structure k) Zn_6; section through two atoms of the tetrahedron and the two surface atoms of the bicapped tetrahedral structure, l) Zn_6; section through a surface triangle of the cuboctahedral structure, m) Zn_{13}; section through a six ring and the central atom of the cuboctahedral structure, n) Zn_{13}; o) Hg_{13}.

it. This kind of behavior is familiar from highly strained covalent molecules [32]. The system bends the bonds in order to reduce the strain due to the incorporation of *s-p* hybrid-orbitals which favor angles of $> 60°$. The situation remains similar for the trigonal bipyramidal structure where we have to distinguish between axial and equatorial bonds. Figures 4f,g show the different covalent contributions in the case of Zn_5. ELF shows a larger covalent contribution for the equatorial than for the axial bond in perfect agreement with the corresponding bond distances. The largest interatomic contributions are beside the equatorial axes. Again the covalency of the equatorial bonds decreases from $Zn > Cd \approx Hg$ (Figs. 4h,i). For the octahedral structure ELF behaves quite similarly for all the elements. Figures 4j,k show sections through the center of the Zn_6 cluster, respectively, a triangular surface. There is a distinct saddle point with vanishing ELF value between all the atoms. The bicapped tetrahedral structure (Figs. 4l) shows larger covalent contributions among the atoms which form the tetrahedron. In order to give an outlook to what happens for larger clusters we present ELF for the cuboctahedral structure of Zn_{13} (Figs. 4m,n) and Hg_{13} (Fig. 4o). The bond lengths have been optimized using the small basis set described in reference [27]. Reference calculations for Hg_4 showed a significantly too long bond length for the small basis set [27]. We have therefore used corrected bond lengths for the cuboctahedral structure (Zn_{13} $R_e = 3.20$ Å; Hg_{13} $R_e = 3.31$ Å). The scaling factor has been obtained from the corresponding calculations for the tetrahedral structure. Although the distance between neighboring surface atoms and the central atom is identical, we obtained different covalent contributions for Zn_{13}. The ELF value between surface atoms is noticeable larger than between a surface atom and the central atom. For Hg_{13} the saddle points between the atoms do not show such a refinement. The covalent contributions are rather weak and we are still quite a bit away from the covalent region. Further studies on even larger clusters are necessary to investigate the transition region and to figure out the differences between the group 12 elements.

2.2 Ionization potentials and electron affinities

Important properties from a theoretical point of view are the ionization potential (IP) and the electron affinity (EA)

of a cluster. They are experimentally accessible and provide a direct measure for the type of bonding involved in a cluster. Two different kinds of experiments, photoionization [6] and electron-impact ionization [4,10] mass spectroscopy, have been performed for neutral Hg clusters. Both methods yield results in perfect agreement for large clusters. For clusters with $2 \leq n \leq 6$ only electron-impact IPs have been reported in the literature [4]. An exception is Hg_2 for which a photoionization IP of 9.1 eV [33] has been measured, *i.e.*, a value 0.3 eV lower than the corresponding electron-impact IP. Conversely, for Cd clusters both photoionization and photoelectron experiments [1] are reported in the literature.

Care has to be taken when comparing theory and experiment due to possible structural changes of the cluster which may occur in the course of experiment. Especially for small clusters the equilibrium structures of the neutral and charged species differ significantly. It is crucial for any meaningful comparison to take this into account. The time scale relative to nuclear motion, on which the ionization process takes place together with these structural differences determines the outcome of the experiment. In photoelectron spectroscopy the incident photon has an energy well above the threshold which makes the ionization process very fast and definitely vertical [34]. No details about the actual time scales for electron-impact and photoionization processes can be found in the experimental literature. They are generally classified as *very fast to very slow* [34]. Nevertheless, these experiments are usually discussed in terms of vertical transitions [9,35,36]. A partial justification can be given by comparison with photoelectron spectra for selected Cd [1–3] and Hg [3,9, 13] clusters. Fast processes compared to nuclear motion are at best represented in theory by vertical IPs where the nuclei are kept fixed. This can be seen by comparing the potential energy curves of Hg_2 ($R_e = 3.77$ Å) and Hg_2^+ ($R_e = 2.81$ Å) (see ref. [27] for details) which clearly shows that the Franck-Condon factors for adiabatic transitions must be very small. The difference between vertical and adiabatic IPs can be quite large for small clusters, *e.g.*, for Hg_2 it amounts to 0.6 eV. In contradiction to this kinds of reasoning are photoionization experiments for rare gas dimers (for a review see ,*e.g.*, Ref. [34,37]), where the qualitative bonding picture is very similar to group 12 dimers. In this case it has been proven that photoionization experiments measure the adiabatic IP, whereby the transition probably takes place via a metastable highly excited Rydberg state followed by autoionization.

A further complication arises from finite temperature effects on the IPs of hot clusters [35]. Without anticipating a more thorough discussion of the vibrational spectra in the next section we want to mention that the vibrational modes are rather soft. The harmonic vibrational frequencies ω for small Cd and Hg clusters vary between 15 cm^{-1} and 50 cm^{-1}. As a consequence, there is a finite probability to encounter nuclei of hot clusters far away from the equilibrium positions. The energies required for vertical ionizations may therefore scatter considerably. In order to estimate the width of this effect it is necessary to take the nuclear motion into account. A combined treatment of highly correlated large-scale *ab initio* electronic structure methods with classical dynamics for the nuclei is far beyond our computational facilities. Since we are mainly interested in qualitative estimates, the application of an effective model potential to mimic the interatomic interactions seems to be justifiable. We discuss the construction of such a potential in the following sections.

In a previous publication [27] we have already discussed the IPs of Hg clusters. We obtained a reasonable agreement with experiment by assuming vertical transitions (see Fig. 5). A perfect agreement between theory and experiment cannot be expected due to finite temperature effects discussed above. We also have to admit that our two-valence electron PP approach is not perfectly accurate as can be seen from the atomic IP in Fig. 5. The discrepancies for Hg are therefore within the uncertainties of our approach.

The situation is somewhat different for Cd clusters where the difference between calculated vertical IPs and experiment is much larger. Already for the dimer we got a vertical IP which is 0.5 eV larger than the experimental result. For the trimer the discrepancy increases even further to 0.9 eV. This is not acceptable from the theoretical point of view and we compared our results for the dimer and trimer with calculations using a more accurate small-core PP, which has already been applied by Yu and Dolg [25] to the atom and the dimer. Correlating the $4s$, $4p$, $4d$, $5s$ shells they performed CCSD(T) calculations using very large basis sets. The first and second atomic IP and dipole polarizability as well as the vibrational frequency and binding energy of the dimer were found to be in excellent agreement with experiment. Applying the same procedure we obtained an IP for the dimer which agrees within 0.1 eV with our previous calculation. For the trimer we restricted our calculations to the CCSD level. Correlating the $4d$, $5s$ shells only we obtained again a good agreement with our large-core PP calculation. Therefore, insisting on a fast vertical ionization process out of the equilibrium structure does not seem to be appropriate any more. A possible solution to this problem might be given by assuming a slow adiabatic transition in the case of photoionization experiments at the threshold. We have already mentioned that for Hg_2 the photoionization IP is half-way between the vertical and adiabatic IP. Taking into account that Hg is nearly twice as heavy as Cd, it seems to be plausible to assume that Cd clusters undergo an almost adiabatic transition in photoionization experiments. We have calculated the equilibrium properties of Cd_2^+ using both small- and large-core pseudopotentials. The calculated spectroscopic properties obtained with small- (large-) core pseudopotentials are $D_e = 1.39$ eV, $R_e = 2.82$ Å, $\omega_e = 124$ cm^{-1} ($D_e = 1.35$ eV, $R_e = 2.91$ Å, $\omega_e = 117$ cm^{-1}). The corresponding adiabatic IP of 7.59 eV (7.45 eV) is in better agreement with experiment (7.7 eV) than the vertical one. It is not straightforward to determine the adiabatic IPs of the larger clusters since it requires an unconstrained structure optimization of the cations. We performed such
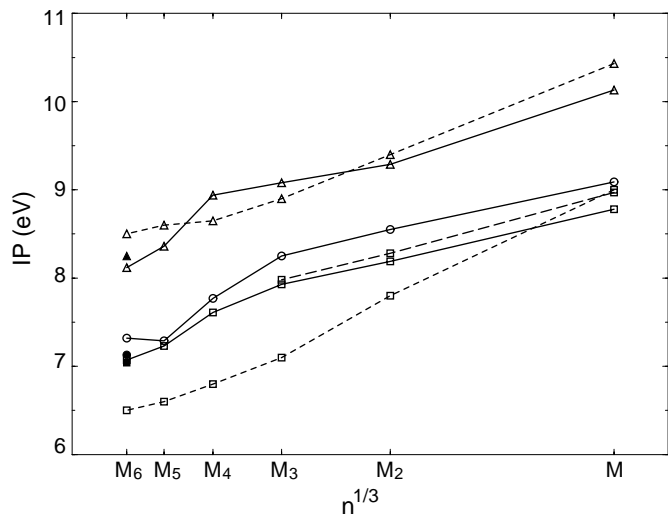
Fig. 5. Vertical ionization potential (eV) for Zn ○, Cd □ and Hg △ clusters. Solid (dashed) lines refer to CCSD(T) calculations using the large (small) core PP. The short-dashed lines are experimental results taken from references [1,4]. The filled symbols refer to the bicapped tetrahedral structure of M_6.

an optimization for Cd_3^+ where we obtained a linear structure with $D_{\infty h}$ symmetry. The adiabatic IP (6.85 eV) is in better agreement with experiment (7.1 eV) than the vertical IP (7.93 eV). Unfortunately the validity of this explanation is questioned by the larger clusters Cd_4, Cd_5 and Cd_6 for which the IPs have been derived from photoelectron spectra [1], which definitely correspond to vertical excitations [34]. Both photoionization and photoelectron experiments have been performend for Cd_6. The derived IPs are in perfect agreement and 0.6 eV lower than our calculated value. An inspection of the actual spectra (Fig. 6 in ref. [2]) shows that our calculated vertical IPs are at the center of the peaks for Cd_5 and Cd_6.

For the purpose of comparison it is most important to choose a consistent measure for all the group 12 elements. Regardless of what has been measured in experiment we have taken the vertical IPs to discuss the behavior of group 12 elements with increasing cluster size. The vertical IPs for Zn, Cd and Hg clusters with up to six atoms are shown in Figure 5. From the IP point of view, Zn, Cd and Hg behave qualitatively very similarly. Moreover, Zn and Cd agree even quantitatively. The decrease in the IP between three and six atoms is 0.93, 0.86 and 0.96 eV for Zn, Cd and Hg, respectively. Taking the difference between the vertical ionization potential and electron affinity (EA), we can define a cluster analog to the band gap IP − EA in solid state physics. On the way to the metallic regime the band gap shrinks to zero. For the small clusters considered in the present work the EAs are listed in Tables 1 to 4. The vertical EAs of the group 12 element clusters are close together and range between 0.4 and 0.8 eV for the tetrahedral, trigonal bipyramidal, respectively octahedral structure. The predominant effect for closing the gap is therefore the strong decrease of the IP with increasing cluster size.

While the present paper was in revision, a publication of Busani *et al.* [38] appeared where they report on photoelectron spectra of negatively charged Hg clusters. The EAs for the small clusters derived in this work are considerably larger than our results. Again care has to be taken in comparing theory and experiment. The photoelectron spectra measure vertical excitations from the equilibrium structure of the negatively charged cluster which may differ significantly from the neutral structure. In order to demonstrate this we have optimized the structure of the negatively charged species Hg_3^-, Hg_4^-. A bond length contraction of 0.36 Å, respectively, 0.15 Å has been obtained for the two species. It is the vertical IP of 0.29 eV, respectively, 0.46 eV for the negatively charged clusters which has to be compared with experiment. Since the unpaired electron occupies a p-type orbital, spin-orbit effects lead to a further stabilization of the negatively charged species by approximately 0.05 eV.

2.3 Vibrational frequencies

Even for a small number of atoms there are plenty of possible structures which may represent local minima on the energy hypersurface. In order to decide whether or not there is a local minimum, it is necessary to determine the harmonic vibrational frequencies and to check if any of these is zero or takes an imaginary value. The structures discussed above have been selected under the assumption that the dominant interaction have no preferred spatial orientation. This is not valid for covalent contributions. Clusters with mainly covalent interactions like alkali metal clusters prefer completely different structures [39]. Therefore it seems to be desirable to check the correctness of our assumptions. The calculation of vibrational frequencies requires the second derivatives of the energy expectation value with respect to the coordinates. This can be done in principle for nearly all kinds of wave functions including the CC method. In practice, it requires a great deal of effort and existing programs have not been made available to the public. At present, second derivatives for HF wave functions are the only ones available; however, for our application HF is not sufficient since the structures of these clusters strongly depend on electron correlation. Additional complications with respect to energy derivatives are caused by the use of CPPs for which an analytic derivatives program has not yet been developed. The only remaining possibility is to calculate the required second derivatives numerically. Fortunately all of our clusters are highly symmetric, we can therefore use group theory to reduce the computational effort considerably (see, *e.g.*, the authoritative monograph of Wilson, Decius, and Cross [40]). The whole problem can be decomposed into one- and two-dimensional independent subproblems for which the required second derivatives can be calculated numerically (cf. the section on computational details below). The calculated vibrational frequencies are listed in Tables 1 to 4. At first we have to notice that all frequencies are real, *i.e.*, all of our structures represent real minima
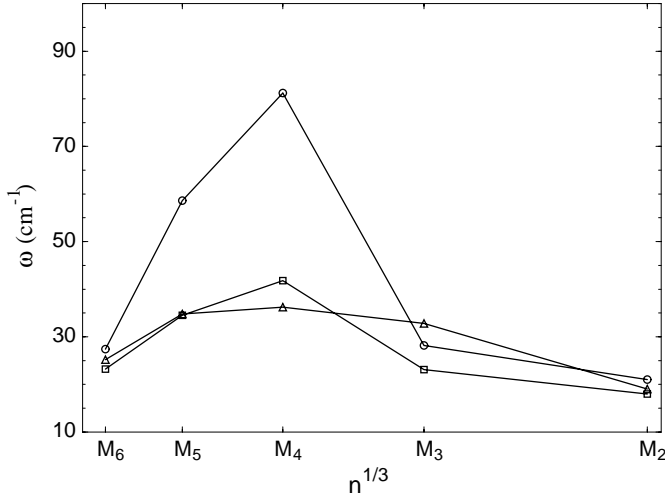
Fig. 6. Averaged vibrational frequencies (cm^{-1}) for Zn $\bigcirc$, Cd $\square$ and Hg $\triangle$ clusters.

on the energy hypersurface. Averaging over all the vibrational modes ω_γ taking into account the degeneracies d_γ we define the averaged vibrational frequency

$$\overline{\omega} = \frac{\sum_\gamma d_\gamma \omega_\gamma}{\sum_\gamma d_\gamma} \qquad (4)$$

for each cluster. Figure 6 shows the dependence of the averaged vibrational frequency on the cluster size. We just want to stress the close similarity between Cd and Hg as well as the sharp increase between Zn_3 and Zn_4. The range of vibrational modes starts to increase for five and six atoms. Especially the soft modes can give some hints concerning the liquidizing of the clusters. Although the cohesive energy for the trigonal bipyramidal structures is more than a factor of three larger than for the dimers, there are E' modes with vibrational frequencies close to that of the dimer. Liquidizing may take place along these modes, but the clusters are too small for any definite treatment of this subject.

2.4 Effective interaction potentials

Besides the electronic properties of group 12 clusters it would be interesting to study the dynamical behavior of these systems. With increasing temperature the systems undergo a phase transition to a liquid state and finally decompose into fragments. The structural features of the liquid state are of special interest since experiments have been performed for hot liquid clusters only. This applies especially to small and medium sized clusters, where the electronic properties are more sensitive to structural changes than to the large ones. The basic ingredient of every simulation studying this feature is an effective interaction potential between the atoms. For van der Waals interacting rare gas clusters such potentials have been determined with very high accuracy. Unfortunately the situation is completely different for group 12 and the related

group 2 clusters. The fundamental problem in adjusting an effective potential is the change of the type of bonding with the size of the cluster. Although we can calculate the potential energy curve for the dimers with very high accuracy [25,41], it makes not much sense to apply it to larger clusters since the covalent contributions are not taken into account. There are several examples in the literature (see, *e.g.*, refs. [42,43]) where effective potentials have been determind from solid state properties. Such potentials are useful for the simulation of large clusters which already show a metallic type of behavior, but they are less appropriate for small and medium sized clusters. Since we are especially interested in this regime, we tried to get some indications for the construction of the potentials from our calculations for small clusters. In the present work we restricted ourselves to two-body interactions. This is not sufficient for accurate simulations which require at least three-body terms. The deficiencies of the two-body approach must remain within acceptable limits in order to be applicable in an actual simulation.

The basic ingredients we can rely upon are the optimized structures, cohesive energies and harmonic vibrational frequencies obtained from our calculations. We have chosen a simple ansatz for our potential

$$V_{ij}^{(2)} = -D(1 + a_2\rho_{ij})\exp(-a_2\rho_{ij}) \qquad (5)$$

with the scaled interatomic distance

$$\rho_{ij} = (r_{ij} - r_e)/r_e. \qquad (6)$$

Such a potential has already been applied as a two-body part for group 2 clusters [42]. For the dimer the parameters D, r_e have a simple interpretation in terms of dissociation energy and equilibrium bond length. The parameter a_2 is related to the vibrational frequency via $\omega_e = a_2\sqrt{2D\mu}/r_e$, with μ denoting the reciprocal mass of the atoms.

The optimization of the parameters has been performed using a least-squares fit,

$$\sigma^2 = w_1(D_e^{\text{opt}} - D_e)^2 + w_2\sum_i(R_i^{\text{opt}} - R_i)^2$$

$$+ w_3\sum_\gamma d_\gamma(\omega_\gamma^{\text{opt}} - \omega_\gamma)^2 \qquad (7)$$

with respect to the structure parameters (R_i), cohesive energy (D_e) and vibrational frequencies (ω_γ) obtained from CCSD(T) calculations. The weight factors w_i where chosen in such a way that $w_1, w_2 \gg w_3$. We found that an increase of w_3 did not result in any significant improvement of the vibrational frequencies but shifted D_e^{opt} to unreasonable values. Apart from this, the optimized parameters where not sensitive with respect to the w_i. In Tables 1 to 4 we have listed the $D_e^{\text{opt}}, R_e^{\text{opt}}, \omega_i^{\text{opt}}$ calculated from the optimized effective model potentials (MP) together with the corresponding CCSD(T) results. The optimized parameters are listed in Table 5. It can be seen that the MP reproduce D_e, R_e for all clusters with regular polyhedral structure very well. Only the trigonal bipyramidal structure with two significantly different bond lengths cannot

Table 5. Model potential parameters (a.u) D, a_2, r_e and averaged vibrational frequency $\overline{\omega}$ (cm^{-1}).

	D	a_2	r_e	$\overline{\omega}^{a}$
Zn$_2$	0.000808	6.403	7.767	21.0
Zn$_3$	0.001115	6.525	7.095	27.5
Zn$_4$	0.002377	10.007	5.546	78.8
Zn$_5$	0.001807	9.407	6.094	58.8
Zn$_6$	0.001131	5.873	6.897	25.7
Cd$_2$	0.001066	6.451	7.994	18.0
Cd$_3$	0.001494	6.390	7.427	22.7
Cd$_4$	0.002096	8.497	6.538	40.6
Cd$_5$	0.001854	7.911	6.713	34.7
Cd$_6$	0.001455	6.250	7.319	22.3
Hg$_2$	0.001617	6.582	7.124	19.0
Hg$_3$	0.002250	8.699	6.633	31.8
Hg$_4$	0.002892	8.298	6.331	36.0
Hg$_5$	0.002772	8.389	6.332	35.7
Hg$_6$	0.002284	6.764	6.713	24.6

[a] Calculated from equation (8).

be reproduced by our approach. Actually it cannot be expected that our simple two-body MP is capable to do so since R_q, R_x cannot deviate too much from r_e without being energetically very unfavorable. Instead of this, we found that $R_q^{\text{opt}} = R_x^{\text{opt}}$ is close to the mean bond distance in the cluster. The vibrational frequencies are well reproduced in the average. The absolute mean differences are 12, 6 and 5 cm^{-1} for Zn, Cd and Hg, respectively. Much better agreement has been obtained for the averaged vibrational frequencies $\overline{\omega}$ for which the agreement is usually close to 1 cm^{-1}. Summing up, it may be said that within our simple ansatz for the effective potential we can reproduce the equilibrium properties of the clusters with reasonable accuracy. A further improvement requires the incorporation of three-body interactions [42] into the MP. Like for the two-body potential one has to adjust the parameters to the size of the clusters. Such a procedure encounters difficulties due to the large number of parameters involved compared to the few available properties of a cluster. Within the present work we are mainly concerned with a qualitative study of the properties of MPs for small group 12 clusters. Therefore we have neclected three-body interactions entirely. Another problem concerns the correct description of the anharmonicity of the MP. It is not taken into account in the adjustment of the parameters which relies only on the part of the energy hypersurface close to the equilibrium structure. Nevertheless, the anharmonicity is very important for the intended application. It is fixed by our simple ansatz for the MP which can be justified in a quantitative manner at least for the dimers. We have compared the whole MP and CCSD(T) potential energy curves and found an excellent agreement over the whole range. Especially the anharmonic long range parts are well reproduced.
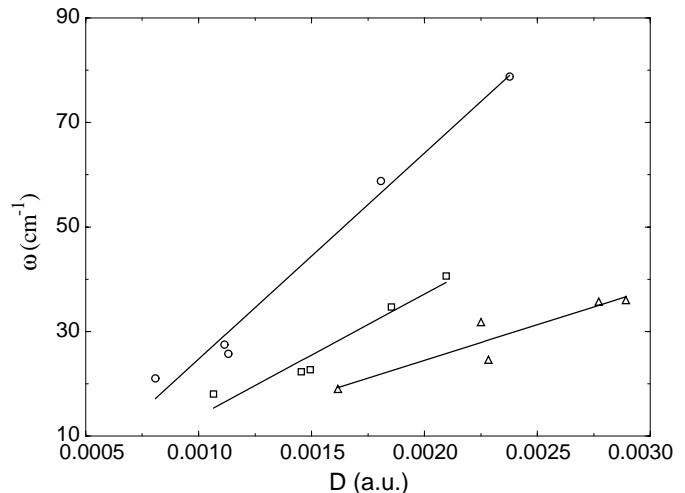

Fig. 7. Averaged vibrational frequencies (cm^{-1}) *versus* the model potential parameter D for Zn $\bigcirc$, Cd $\square$ and Hg $\triangle$ clusters. Linear regressions have been performed through the data points.

We have checked the consistency of our MPs by performing unconstrained structure optimizations using a simulated annealing algorithm [44]. The optimization has been repeated several times with initially randomly distributed atoms in a box. For $n = 4, 5$ only the tetrahedral, respectively the trigonal bipyramidal structure emerged in the optimization. In agreement with our previous assumption we obtained for $n = 6$ both the octahedral and the bicapped tetrahedral structure.

The calculation of vibrational frequencies using the CCSD(T) method requires a considerable numerical effort which can be done for small highly symmetrical clusters only. In order to study the dynamics of larger systems, it is desirable to find a simple scaling relation which takes into account the increasing covalent contributions. We propose a compromise between a scaling of all the parameters and an adjustment according to equation (7). The parameters D, r_e can be assigned to the cohesive energy per nearest-neighbors interaction and the averaged distance between nearest neighbors. The third parameter a_2 can be related to the vibrational frequencies. We suggest the relation

$$\overline{\omega} = \frac{a_2}{r_e}\sqrt{2D\mu}, \tag{8}$$

which is an extension of the corresponding exact relation for the dimer. The $\overline{\omega}$ obtained from equation (8) (see Tab. 5) are in excellent agreement with the CCSD(T) values. By inspection of our data we found a nearly linear relationship of the form $D \sim \overline{\omega}$. In Figure 7 we plotted D *versus* $\overline{\omega}$ for the group 12 elements. At least for Zn, Cd the linear relationship seems to be appropriate and even for Hg it seems to be acceptable. To generate a MP for larger clusters we have to know the bond distances and cohesive energies. The optimization of bond distances becomes very expensive but we have a lower bound given by the bulk value. Bond distances for Hg$_{13}$, Hg$_{15}$ have already been optimized and it should be possible to apply some simple

scaling relation to connect to the bulk distance. Cohesive energies can be obtained from QMC calculations which can be applied to even larger clusters.

3 Conclusions

We have performed CCSD(T) calculations for small group 12 clusters with up to six atoms using large-core relativistic PPs and CPPs. The calculated properties include bond lengths, cohesive energies, IPs, EAs and vibrational frequencies. These data have been used to study the covalent contributions to the bonding in these clusters and to reveal the differences between the group 12 elements. To gain further insight into the structure of the bonding we have applied ELF to these systems. ELF is a very useful tool to study local properties of the bonding and to distinguish between various interatomic interactions in a cluster. It does not suffer from basis set dependences like the standard Mulliken population analysis which is inappropriate in the present application due to the large and diffuse basis sets involved. The covalent contributions are most strongly developed for Zn_4 and Zn_5 clusters. There is a remarkably strong increase in stability between Zn_3 and Zn_4 which is less pronounced for Cd and Hg. Actually, we observed a close similarity between Cd and Hg clusters. This contradicts the experimental findings which indicate stronger covalent contributions for Cd. Especially the discrepancies between the calculated and measured IPs for Cd clusters have not been completely resolved. For a better comparison to experiment, it is highly desirable to take into account finite temperature effects on the structure of these clusters. As a first step in this direction we have adjusted two-body MPs using CEs and vibrational frequencies obtained from our CCSD(T) calculations. We further suggest a simple scaling relation for the generation of MPs for larger clusters which incorporate changes in the covalent contributions with the cluster size. The MPs can be used in molecular dynamics simulations to study at least in a semi-quantitative manner the melting of these clusters. The resulting structural information can in turn be used to study their influence on electronic properties like IPs.

4 Computational details

4.1 Pseudopotentials and valence basis sets

As already outlined above, the application of large-core PPs is essential for the present work in order to keep the computational effort within reasonable limits. We have used two-valence electron relativistic PPs [26,45] which provide an efficient way to incorporate scalar relativistic effects in the calculations. Relativistic effects become increasingly important for Zn, Cd, Hg and cannot be neglected in a comparative study for these elements. Beyond that core-valence correlation plays an essential role in the bonding of these systems [23,25]. This has been taken into
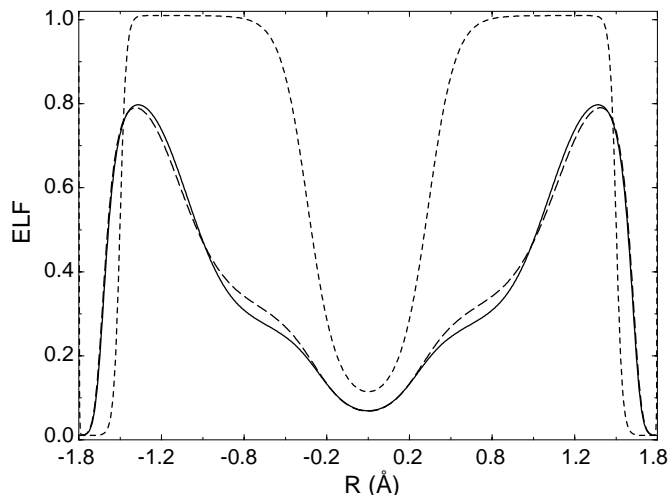

Fig. 8. The ELF of Hg_2 along the interatomic axes obtained from large (dashed line) and small (long-dashed line) core PP calculations. A corrected ELF (solid line) has been obtained by adding the $5s$, $5p$, $5d$ core orbitals to the pseudo-valence orbitals without orthogonalization.

account by using CPPs [46,47]. We have used large uncontracted valence basis sets $(6s6p5d3f1g)$ for $n = 3, 4$ which were reduced to $(6s6p3d2f1g)$ for $n = 5, 6$. Further details concerning the basis sets and the reduction of the polarization functions are given in previous publications [26, 27]. All the calculations reported in this work have been done using the MOLPRO [48–50] program package.

4.2 A technical remark concerning ELF

In principle the ELF is based on quantities accessible from experiment [51]. Since we are doing valence-only calculations including only the highest s shell, this does not remain valid any more. The underlying d shells are not well separated from the s shell. The ELF obtained from our valence-only calculations looks therefore quite different from the ELF obtained from an all-electron calculation or a hypothetical experiment [51]. This is not a real problem in our application since the physical content of ELF remains unchanged in a valence-only calculation. We are only interested in the relative differences of ELF between clusters of different structure or elemental composition. Using the same type of PP in all of our calculations permits a consistent interpretation of our results. However care has to be taken when comparing ELF obtained with different types of PPs. In order to do this, one has to attach the remaining core orbitals to the calculation with the larger core. This can be done only in an approximate way because of the differences in the nodal structure between pseudo-valence orbitals obtained with different kinds of PPs. Figure 8 shows the effect of the core orbitals in the case of Hg_2. The ELF obtained with two and twenty-valence electron PP look quite different. Adding core orbitals we obtain a good agreement between both calculations. This has also been done for larger clusters with the same result. We have renounced to add the

$$F^{(\gamma)} \approx \frac{-\left[E(2S^{(\gamma)}) + E(-2S^{(\gamma)})\right] + 16\left[E(S^{(\gamma)}) + E(-S^{(\gamma)})\right] - 30E(0)}{12S^{(\gamma)2}} \tag{12}$$

$$F_{qx}^{(\gamma)} \approx \frac{E(S_q^{(\gamma)}, S_x^{(\gamma)}) + E(-S_q^{(\gamma)}, -S_x^{(\gamma)}) - E(S_q^{(\gamma)}, -S_x^{(\gamma)}) - E(-S_q^{(\gamma)}, S_x^{(\gamma)})}{4S_q^{(\gamma)} S_x^{(\gamma)}} \tag{13}$$

core orbitals since this introduces additional features into ELF which are not important in the present context.

4.3 Normal coordinate analysis

The study of vibrational structures of highly symmetrical molecules is one of the classical examples for the application of group theory in physics [40]. We applied a standard procedure based on symmetry-adapted internal coordinates which will be briefly oulined in the following. The whole procedure is described in full detail for example in the book of Wilson, Decius and Cross [40]. We have used the nearest-neighbor distances as internal coordinates. The corresponding displacement coordinates are denoted by S_i. With the exception of the trigonal bipyramidal structure we have therefore only one set of internal coordinates for each structure. Every set spans a reducible representation of the corresponding point group. Taking an arbitrary element S_1 of the set we can easily construct symmetry-adapted orthogonal internal coordinates using the formula

$$S^{(\gamma)} = N_\gamma \sum_R \chi_R^{(\gamma)} RS_1 \,, \tag{9}$$

where the sum runs over all elements R of the group and $\chi_R^{(\gamma)}$ is the character of the group element in the corresponding irreducible representation. The $S^{(\gamma)}$ depends on the choice of S_1 if the dimension d_γ of the irreducible representation is greater than one. It is sufficient to consider an arbitrary single representative since the resulting secular equation blocks into d_γ identical subsystems. In the case of the trigonal bipyramidal structure, where two different sets of internal coordinates (equatorial $S_q^{(\gamma)}$ and axial $S_x^{(\gamma)}$ distances) belong to the same irreducible representation of $d_\gamma = 2$, care has to be taken that the two representatives obey the same transformation properties. In our applications the force constant matrix elements appear only in their diagonal form

$$F^{(\gamma)} = \frac{\partial^2 E}{\partial S^{(\gamma)2}} \tag{10}$$

with the exception of the trigonal bipyramidal structure where we also have nondiagonal coupling elements

$$F_{qx}^{(\gamma)} = \frac{\partial^2 E}{\partial S_q^{(\gamma)} \partial S_x^{(\gamma)}} \,. \tag{11}$$

We have used the five-point numerical differentiation formula

see equation (12) above

for the diagonal matrix elements with $S_i = 0.1$ bohr and the four-point formula

see equation (13) above

for the nondiagonal parts of the trigonal bipyramidal structure. The relatively large value for the displacement coordinates is necessary due to the weak bonding. The change in energy has to be large enough compared to the numerical accuracy of the total energy. We performed some tests on the numerical accuracy of our procedure from which we expect errors of less than 1 cm^{-1} for the vibrational frequencies. Given the force matrix elements, it is an easy task so solve the secular equation $\mid GF - \omega^2 I \mid$ which factors into one- and two-dimensional subsets. The secular equation contains the G-matrix related to the kinetic energy, its matrix elements can be obtained using the tables and rules given in reference [40].

References

1. M. Ruppel, K. Rademann, Chem. Phys. Lett. **197**, 280 (1992).
2. K. Rademann, M. Ruppel, B. Kaiser, Ber. Bunsenges. Phys. Chem. **96**, 1204 (1992).
3. K. Rademann, J. Non-Cryst. Solids **156-158**, 794 (1993).
4. B. Cabaud, A. Hoareau, P. Melinon, J. Phys. D **13**, 1831 (1980).
5. C. Bréchignac, M. Broyer, Ph. Cahuzac, G. Delacretaz, P. Labastie, L. Wöste, Chem. Phys. Lett. **120**, 559 (1985).
6. K. Rademann, B. Kaiser, U. Even, F. Hensel, Phys. Rev. Lett. **59**, 2319 (1987).
7. C. Bréchignac, M. Broyer, Ph. Cahuzac, G. Delacretaz, P. Labastie, J.P. Wolf, L. Wöste, Phys. Rev. Lett. **60**, 275 (1988).
8. K. Rademann, Ber. Bunsenges. Phys. Chem. **93**, 653 (1989).
9. K. Rademann, B. Kaiser, T. Rech, F. Hensel, Z. Phys. D **12**, 431 (1989).
10. H. Haberland, H. Kornmeier, H. Langosch, M. Oschwald, G. Tanner, J. Chem. Soc. Faraday Trans. **86**, 2473 (1990).

11. H. Haberland, H. Langosch, Z. Phys. D **19**, 223 (1991).
12. B. Kaiser, K. Rademann, Z. Phys. D **19**, 227 (1991).
13. B. Kaiser, K. Rademann, Phys. Rev. Lett. **69**, 3204 (1992).
14. K. Rademann, O. Dimopoulou-Rademann, M. Schlauf, U. Even, F. Hensel, Phys. Rev. Lett. **69**, 3208 (1992).
15. H. Haberland, B. von Issendorff, J. Yufeng, T. Kolar, Phys. Rev. Lett. **69**, 3212 (1992).
16. B. Lang, A. Vierheilig, E. Wiedenmann, H. Buchenau, G. Gerber, Z. Phys. D **40**, 1 (1997).
17. G.M. Pastor, P. Stampfli, K.H. Bennemann, Europhys. Lett. **7**, 419 (1988).
18. M.E. Garcia, G.M. Pastor, K.H. Bennemann, Phys. Rev. Lett. **67**, 1142 (1991); Phys. Rev. B **48**, 8388 (1993).
19. G.M. Pastor, K.H. Bennemann, in *Clusters of Atoms and Molecules*, edited by H. Haberland, Vol. I (Springer, Berlin, 1994) p. 86.
20. P.P. Singh, K.S. Dy, Z. Phys. D **17**, 309 (1990).
21. F. Yonezawa, H. Tanikawa, in *Computational Physics as a New Frontier in Condensed Matter Research*, edited by H. Takayama, M. Tsukada, H. Shiba, F. Yonezawa, M. Imada, Y. Okabe (The Physical Society of Japan, 1995) p. 77.
22. D.C. Patton, M.R. Pederson, Phys. Rev. A **56**, 2495 (1997).
23. M. Dolg, H.-J. Flad, J. Phys. Chem. **100**, 6147 (1996).
24. H.-J. Flad, M. Dolg, J. Phys. Chem. **100**, 6152 (1996).
25. M. Yu, M. Dolg, Chem. Phys. Lett. **273**, 329 (1997).
26. F. Schautz, H.-J. Flad, M. Dolg, Theor. Chem. Acc. **99**, 231 (1998).
27. M. Dolg, H.-J. Flad, Mol. Phys. **91**, 815 (1997).
28. A. Bartelt, J.D. Close, F. Federmann, N. Quaas, J.P. Toennies, Phys. Rev. Lett. **77**, 3525 (1996).
29. A.D. Becke, N.E. Edgecombe, J. Chem. Phys. **92**, 5397 (1990).
30. A. Savin, A.D. Becke, J. Flad, R. Nesper, H. Preuss, H.G. von Schnering, Angew. Chem. **103**, 421 (1991); Angew. Chem. Int. Ed. Engl. **30**, 409 (1991).
31. A. Savin, R. Nesper, S. Wengert, T.F. Fässler, Angew. Chem. **109**, 3001 (1997); Angew. Chem. Int. Ed. Engl. **36**, 1808 (1997).
32. A. Savin, H.J. Flad, J. Flad, H. Preuss, H.G. von Schnering, Angew. Chem. **104**, 185 (1992); Angew. Chem. Int. Ed. Engl. **31**, 187 (1992).
33. S.H. Linn, C.L. Liao, C.X. Liao, J.M. Brom Jr., C.Y. Ng, Chem. Phys. Lett. **105**, 645 (1984).
34. H. Haberland, in *Clusters of Atoms and Molecules*, edited by H. Haberland, Vol. I (Springer, Berlin, 1994) p. 374.
35. W.A. de Heer, Rev. Mod. Phys. **65**, 611 (1993).
36. P.M. Guyon, J. Berkowitz, J. Chem. Phys. **54**, 1814 (1971).
37. C.Y. Ng, in *Advances in Chemical Physics*, edited by I. Prigogine, S.A. Rice, Vol. LII (Wiley, 1983) p. 263.
38. R. Busani, M. Folkers, O. Cheshnovsky, Phys. Rev. Lett. **81**, 3836 (1998).
39. V. Bonačič-Koutecký, P. Fantucci, J. Koutecký, in *Clusters of Atoms and Molecules*, edited by H. Haberland, Vol. I (Springer, Berlin, 1994) p. 15.
40. E.B. Wilson Jr., J.C. Decius, P.C. Cross, *Molecular Vibrations* (McGraw-Hill, 1955).
41. J. Koperski, J.B. Atkinson, L. Krause, J. Mol. Spectrosc. **184**, 300 (1997).
42. J.E. Hearn, R.L. Johnston, J. Chem. Phys. **107**, 4674 (1997).
43. R. Ramprasad, R.G. Hoagland, Modelling Simul. Mater. Sci. Eng. **1**, 189 (1993).
44. W.H. Press, B.P. Flanery, S.A. Teukowsky, W.T. Vetterling, *Numerical Recipes* (Cambridge University Press, 1986).
45. W. Küchle, M. Dolg, H. Stoll, H. Preuss, Mol. Phys. **74**, 1245 (1991).
46. W. Müller, J. Flesch, W. Meyer, J. Chem. Phys. **80**, 3297 (1984).
47. P. Fuentealba, H. Preuss, H. Stoll, L. von Szentpály, Chem. Phys. Lett. **89**, 418 (1982).
48. MOLPRO is a package of *ab initio* programs written by H.-J. Werner and P.J. Knowles, with contributions from J. Almlöf, R.D. Amos, M.J.O. Deegan, S.T. Elbert, C. Hampel, W. Meyer, K. Peterson, R.M. Pitzer, A.J. Stone, and P.R. Taylor.
49. C. Hampel, K. Peterson, H.-J. Werner, Chem. Phys. Lett. **190**, 1 (1992).
50. P.J. Knowles, C. Hampel, H.-J. Werner, J. Chem. Phys. **99**, 5219 (1993).
51. M. Kohout, A. Savin, J. Comp. Chem. **18**, 1431 (1997).